FIBRONECTIN NETWORK INFLUENCES ENDOTHELIAL CELL MIGRATION DURING VASCULAR MORPHOGENESIS IN A BREAST CANCER MODEL

by
Kimberly Ellis

A thesis submitted to Johns Hopkins University in conformity with the requirements for the degree of Master of Science in Engineering

Baltimore, Maryland
May, 2014

Abstract

Angiogenesis, the formation of new blood vessels from pre-existing vessels, is a major research topic in the biomedical field due to its role in regenerative medicine, tissue engineering, and cancer development, growth, and metastasis. This process is driven by the demand for oxygen and nutrients from the surrounding tissues, and is heavily regulated by the extracellular matrix (ECM). The ECM is a non-cellular, complex network made up of fibrous proteins, growth factors, and signaling molecules. Many researchers have studied the individual constituents of this protein rich matrix and the specific roles they play during angiogenesis hoping to find a potential target for cancer treatments.

Previous research conducted in our lab has established fibroblast and breast cancer cell-derived scaffolds as a platform to investigate tumor angiogenesis. This thesis focuses on the influence of the fibronectin network in the cell-derived scaffolds on endothelial cell (EC) migration. We used pUR4B, a fibronectin polymerization inhibitor, and III-11C, the control peptide that has no effect on fibronectin polymerization to manipulate matrix deposition. We also established a line of green fluorescent protein (GFP) tagged EC's using lentiviral GFP. After seeding the GFP ECs on the de-cellularized scaffolds, we tracked the migration of the cells and quantified several migration parameters. Our results showed that the polymerized fibronectin restricts EC migration during angiogenesis. Its function to support the surrounding matrix components and adhesive properties are essential for endothelial cell migration. These findings shed new light on the role of polymerized fibronectin in endothelial cell

migration during angiogenesis, and further prove its potential as a target for future cancer treatment.

Advisor: Dr. Sharon Gerecht

Readers: Dr. Sharon Gerecht and Dr. Honggang Cui

Preface

I would first like to graciously thank Dr. Sharon Gerecht for allowing me to pursue my master's thesis research in her laboratory and providing me with essential guidance on my project. She has not only been an inspiration as a woman in engineering, but her drive and passion for regenerative medicine has motivated me to endlessly pursue my goals. I would also like to acknowledge Dr. Honggang Cui for being on my committee. His input and advice on this project has been very insightful and helpful. In addition, I'd like to thank Dr. Abigail Hielscher for her mentorship through my master's research project. She taught me many experimental techniques I needed to complete my project and has also provided me with several suggestions and indispensible advice on troubling experiments. Without Abby, I would not have been able to complete this thesis.

I would also like to thank all of the members of the Gerecht lab for their support along the way. It was an incredible opportunity to work alongside such brilliant and hard working individuals. They motivated me to work harder everyday, and for that I am truly grateful.

Lastly, I would like to thank my family and friends for their endless acts of encouragement and love during this journey. Their support has played a crucial role in my success and without them I would not be where I am today.

Table of Contents

Abstract ii

Preface iv

Table of Contents v

List of Symbols vi

List of Figures vii

Introduction 1

Materials and Methods 10

Results 17

Discussion 37

Conclusion 44

Future Work 46

References 48

Resume 53

List of Symbols

ECM	Extracellular matrix
HUVEC	Human umbilical vein endothelial cell
NuFF	Neonatal foreskin fibroblast
VEGF	Vascular endothelial growth factor
MMP	Matrix metalloproteinase
GAGs	Glycosaminoglycans
kDa	Kilodalton
MSD	Mean square displacement
GFP	Green fluorescent protein
cm	Centimeter
ml	Milliliter
µl	Microliter
µm	Micron
nm	Nanometer
µg	Microgram
min	Minute
SSC	Side scattering
FSC	Forward scattering
nM	Nanomolar
Fn	Fibronectin
Inhib	Inhibitor

List of Figures

Figure 1: Process of Angiogenesis 1

Figure 2: Cell Migration Parameters 8

Figure 3: Outline of Experimental Steps 17

Figure 4: Phase Contrast Images of Cells in Culture 18

Figure 5: GFP HUVEC Sorting 19

Figure 6: GFP High, GFP Low, and GFP Negative HUVECs 20

Figure 7: pUR4B test on Fibronectin Polymerization 22

Figure 8: Cell Cultures Prior to De-cellularization 23

Figure 9: Cell Tracking Trajectories 25

Figure 10: Total Distance Travelled 27

Figure 11: Net Displacement 28

Figure 12: Average Velocity 30

Figure 13: Interval Velocities 31

Figure 14: Mean Square Displacement 33

Figure 15: Fluorescent Images of HUVECs 12 Hours Post Seeding 35

Introduction

Angiogenesis, the formation of new blood vessels from pre-existing vessels, is a major research topic in biomedical engineering due to its role in regenerative medicine, tissue engineering, and the development, growth, and metastasis of cancerous tissues. In the past decade much has been done to investigate this biological process and acquire an advanced understanding [1]. An increasing demand for a deeper knowledge of this essential biological process as a potential therapeutic target calls for the need to develop tools that mimic the physiological conditions of the microenvironment in which angiogenesis occurs.

Angiogenesis is driven by the needs of avascular and ischemic regions in the body and provides surrounding tissues with oxygen and essential nutrients [2]. It is necessary for healthy tissue development and survival and harmful pathological processes. The angiogenic process consists of a series of events illustrated in **figure 1** [3]. After endothelial cells are activated by signal molecules such as vascular endothelial growth factor (VEGF), dissociation of the basement membrane and ECM occurs. Matrix metalloproteinases (MMPs) are a family

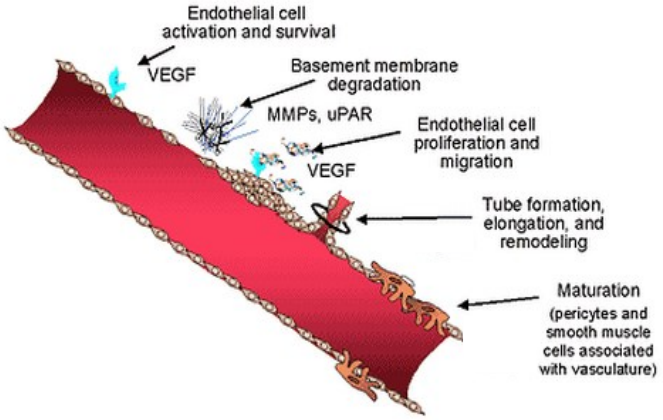

Figure 1: Process of Angiogenesis. Above illustrates the cascade of angiogenic events. Endothelial cells are first activated, following by degradation of the basement membrane. The endothelial cells then proliferate and migrate forming capillary like structures (CLS). Maturation proceeds with the envelopment of pericytes and smooth muscle cells around the newly formed structures [3].

of enzymes that are responsible for this degradation, and allow the migration of endothelial cells through the matrix by "tip" cells. This is followed by proliferation of the trailing endothelial "stalk" cells, which connect the "tip" cell to the pre-existing vessel. After endothelial cells align into cord like structures, they resynthesize the basement membrane and return to their quiescent stage [2]. This sequence of angiogenic events is crucial to normal physiological processes like fetal development [4] and would healing [5], as well as the development of cardiovascular disease [6], and cancer [7].

Angiogenesis is regulated by a balance of "pro" and "anti" angiogenic factors which are responsible for either inducing or inhibiting different steps of the cascade [8]. Some of the most important angiogenic factors include VEGF, angiopoitin-2, and fibroblast growth factor (FGF); some common anti-angiogenic factors are angiostatin and endostatin [9]. There has been significant progress in targeting angiogenic factors, more specifically VEGF, as a therapeutic for cancer treatment. In August of 2004 a VEGF inhibitor, bevacizumab (Avastin), received approval from United States Food and Drug Administration for metastatic colorectal cancer, noted as the first ever anti-angiogenic biologic drug targeting cancer to reach the market [10]. Since its major success, numerous studies and clinical trials have focused on the discovery and administration of new anti-angiogenic therapeutics to target cancer [11]. As the demand increases for discovering new therapeutics to target angiogenic factors in cancer, so does the need to develop a model that mimics the physiological properties of cancerous tissues and its surrounding ECM.

The ECM is a fundamental component of the microenvironment of blood vessels, which contributes more than just a supporting scaffold. Its versatility allows regulation

of all cellular functions essential for angiogenesis including adhesion, migration, proliferation, differentiation, and lumen formation [12]. The ECM is composed of a diverse meshwork of various molecules that influence embedded cells' survival, shape, polarity, and mobility and acts as a "reservoir" regulating the availability and activity of important signaling molecules [13]. The matrix consists mostly of woven protein fibers in a hydrated gel with glycosaminoglycans (GAGs) and proteoglycans [14]. The most common elements of the ECM are laminans, collagens, fibronectin, and elastins. In addition, the ECM also includes non-fibrous proteins like tenascin as well as specific growth factor associated proteins like TGF-β binding proteins. Modifications in the ECM composition and organization are extensively identified in several pathological situations including fibrosis and cancer [15, 16].

Blood vessels are composed of endothelial cells, which stably adhere to the surrounding ECM. Neighboring pericytes and smooth muscle cells support these endothelial cells as stated earlier [12]. Interactions between endothelial cells and the ECM are crucial for vascular development, formation, and maturation. When blood vessels are in their quiescent stage, the ECM consists of high level of laminins, collagen IV, and other highly cross-linked components, which supply a great degree of structural support [17]. However, during angiogenesis the ECM is remodeled by MMPs [18]. This remodeling exposes endothelial cells to different domains of ECM molecules inducing vascular morphogenesis, which otherwise would not have been cued by previous domains of the molecules. Cells are also stimulated to up-regulate the secretion of certain proteins. The angiogenic growth factor VEGF is known to cue endothelial cells to produce new ECM molecules that integrate into this "provisional" matrix [19]. The

remodeled matrix cues endothelial cells to alter their current attachment position and migrate further in to the surrounding microenvironment.

To further understand the specific effects the ECM has on endothelial cells, researchers use a variety of ways to recapitulate the host environment surrounding the endothelial cells during angiogenesis [20]. One of the most common *in vitro* tools currently used to mimic the ECM is Matrigel. It is a soluble laminin and collagen IV-rich basement membrane extracted from mouse tumors, which is known to support the organization of endothelial cells into stable vascular structures [21]. Because of this, it has been widely used to investigate anti-angiogenic therapy targets and has proven much success for this purpose [22-24]. Although Matrigel provides a useful platform to study anti-angiogenic therapies, it has much variation from batch to batch making it difficult to reproduce experiments [25]. It is also costly and temperature sensitive. As a result, researchers use other scaffolds that contain the native, cell-derived ECM components to further investigate anti-angiogenic therapies on vascular morphogenesis. One substance that has been used as an *in vitro* scaffold to study the formation of microvasculature is a fibroblast-derived ECM [20]. Soucy and Romer were the first to prove that a natural fibroblast derived ECM directed vascular growth and development [26]. The cell derived ECM has also been used as a scaffold to study angiogenesis in cancerous tissues. Hielscher and colleagues used a co-culture of human fibroblasts and three different types of breast cancer cells to mimic the breast cancer microenvironment [27]. In addition, they used this scaffold to study the differences in ECM components between the individual breast cancer cell lines and were able to determine the different effects they had on vascular morphogenesis of endothelial cells. These cell-derived scaffolds provide

a sufficient mimetic matrix to study vascular morphogenesis in healthy and cancerous tissues and have potential to be used to study anti-angiogenic molecules. As a result of these advantages, cell-derived scaffolds will be used in experiments described in subsequent sections of this thesis.

In search for an anti-angiogenic drug to target pathological processes, scientists have looked into certain proteins expressed at high levels during angiogenesis. One protein of great interest is fibronectin due to its notable presence in the ECM surrounding developing microvasculature [28, 29]. Fibronectin is a molecule known to be well dispersed throughout the ECM and proves to have an essential role in the morphogenesis of blood vessels during development and in pathological properties, such as cancer [30]. Fibronectin is a fairly large protein varying from 240 to 270 kDa and exists in various isoforms and conformations [12]. There are two forms of fibronectin recognized in the body: one is plasma fibronectin, produced by hepatocytes, which circulates in the blood stream at high concentrations [30]. The second form is cellular fibronectin, which is produced and secreted by cells into tissues where it becomes an integral component of the fibrillar extracellular matrix. Cellular fibronectin interacts with several other ECM molecules and thus acts as a supporting scaffold for the continuous assembly of the matrix. It is also highly interactive with endothelial cells and is known to bind to integrin cell surface receptors through the RGD (Arg-Gly-Asp) motif [30, 31]. Through this binding, fibronectin is capable of transmitting signals to the cells, allowing it to modify cellular behavior.

Several studies have demonstrated the various roles of fibronectin in endothelial cell adhesion and migration during vessel development and sprouting. Fibronectin is

strongly expressed within the matrix surrounding developing blood vessels and is almost undetectable in normal adult blood vessels [12]. Expression of fibronectin in adult organisms is known to occur during pathological angiogenesis in wound healing and various diseases like fibrosis, vascular disease, and cancer [32]. Researchers found that genetic ablation of fibronectin in mice resulted in embryonic lethality with fatal cardiovascular defects. While initial vessel formation occurred, angiogenic sprouting was completely absent, deeming fibronectin's crucial role in the angiogenic cascade [33]. Other researchers have found that astrocyte-deposited fibronectin fibrils guide endothelial cell migration at the angiogenic front [17]. In addition to the angiogenic effect of the fibronectin protein, fibrillogenesis, the polymerization of fibronectin into a network, is observed in the provisional matrix during angiogenesis. By blocking polymerization of fibronectin, scientists have noted a decrease in endothelial cell proliferation and lumen formation in a three-dimensional cell culture model *in vitro* and in the CAM assay *in vivo* [34].

Because fibronectin polymerization has been observed in the ECM during angiogenesis, it could potentially be targeted as an anti-angiogenic therapy. Ho-Yu Chiang and colleagues have studied ECM deposition and vascular remodeling using a fibronectin polymerization inhibitor [35]. They used pUR4B, a recombinant peptide derived from F1 adhesion, to inhibit fibronectin polymerization and determine its effects on vascular remodeling in mice. They showed that fibronectin deposition was drastically decreased in mice that were treated with the inhibitory peptide and proved its importance in vascular remodeling. In addition to these findings, Jane Sottile and Denise Hocking used fibronectin-null cells and discovered that fibronectin polymerization globally

controls the composition and stability of the extracellular matrix and cell-matrix adhesion sites, therefor controlling the signaling cascades that regulate neighboring cell behavior [36]. Although these findings are significant, more research needs to be conducted to further understand the role of this inhibitor during the angiogenic cascade.

To gain a better understanding of the role of polymerized fibronectin in angiogenesis in both healthy tissue development and tumorigenesis, we proposed to study several migration parameters of endothelial cells during the angiogenic process, both in a breast cancer ECM model and in a Neonatal human Foreskin Fibroblast (NuFF)-derived ECM. Cell migration and motility are essential in many physiological and pathological processes like embryogenesis, would healing, inflammation, and metastasis [37]. While many researchers studying angiogenesis in different scaffolds have focused on several cellular and molecular events that occur, very few have quantified the cell motility of endothelial cells during the angiogenic cascade. The migratory pathway of endothelial cells could provide a deeper understanding of angiogenesis and could be used to study ways in which the surrounding microenvironment regulates the cell motility.

Endothelial cell migration involves three major mechanisms including chemotaxis, the directional migration toward a gradient of soluble chemoattractants; haptotaxis, the directional migration toward a gradient of immobilized ligands; and mechanotaxis, the directional migration generated by mechanical forces [38]. Chemotaxis results in the response to growth factors while haptotaxis is due to integrins of the endothelial cells binding to the ECM components [39]. Mechanotaxis is initiated by the shear stress of fluid that passes by the endothelial cells [40]. Since the experiments performed are aimed to study the migration of endothelial cells in static

culture and as a response to matrices of different components, the major mechanism focused on is haptotaxis.

Migrating cells follow a persistent random walk model of which cell speed is a key parameter [41]. Cell speed, or cell velocity is a parameter of interest for our experiments because it quantifies the rate at which the endothelial cells migrate. Another common parameter used to quantify migrating cells is the mean square displacement (MSD) [42]. This parameter is a way to measure the mechanical properties of the environment surrounding the cells as well as their interactions. In addition to these two parameters, path length or total distance travelled and net displacement are also important factors of cell motility and migration [43]. The distance travelled and net displacement provides insight into the directionality of the cells and the interactions between the cells and the surrounding environment. **Figure 2** shows each migration parameter quantified.

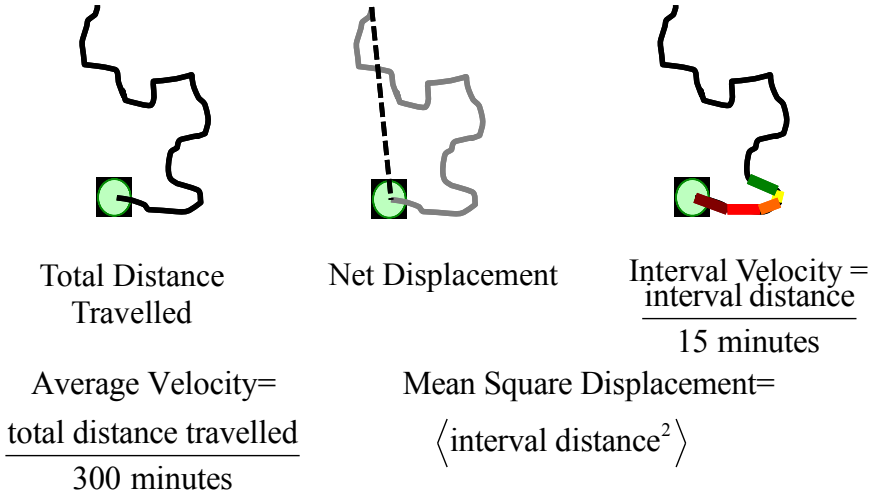

Figure 2: Cell Migration Parameters. Above displays the five cell migration parameters quantified. The total distance travelled quantifies the path length the cell travelled while the net displacement quantifies the distance from the cell's initial position to its final position. The average and interval velocities show the difference in migration rates and the mean square displacement allows comparison of the interval distances for each scaffold.

This quantitative analysis of endothelial cell motility will be useful for determining how each microenvironment affects the migration of endothelial cells as they progress from their quiescent stage into developing microvasculature.

Materials and Methods

Cell lines and culture

The human neonatal foreskin fibroblast (NuFF) cell line was obtained from Global Stem (Rockville, MD) at passage 9. Human umbilical vein endothelial cells (HUVECs) were obtained from Promocell (Heidelberg, Germany). MDA231 were a gift from the Physical Sciences-Oncology Center (PSOC, National Institutes of Health, Bethesda, MD) and were obtained through the laboratory of Dr. Thea Tlsty (University of California, San Francisco, CA). NuFF cells were cultured in Dulbecco's modified Eagle's medium (DMEM; GIBCO, Carlsbad, CA) supplemented with 10% (vol/vol) heat-inactivated fetal bovine serum (FBS; Atlanta Biologicals). HUVECs were cultured in endothelial cell growth medium (ECGM; Promocell) supplemented with ECGM SupplementMix (Promocell). Medium was changed every 2-3 days and passaged after reaching 90% confluency with 0.25% trypsin EDTA (Sigma, Allentown, PA) or 0.05% trypsin EDTA (for HUVECs). All cell lines were maintained at 37°C, 5% CO_2 in a humidified atmosphere.

HUVECs transfection with GFP

HUVECs (at passage 1) were transfected with lentiviral GFP. The cells were plated in a 6-well plate (Cellstar) at $1x10^5$ cells/well. The virus was added at a ratio of 1:100 (vol/vol) virus to HUVEC medium and incubated at 37°C, 5% CO_2 in a humidified atmosphere for 24 hours. The media was changed after the 24-hour viral incubation. The cells were then scrapped off the wells with a 25cm cell scraper (Sarstedt), spun down at 800 rpm for 3 minutes, and suspended in 300µl of phosphate buffer saline (PBS;

GIBCO). This suspension was filtered using a 40-um mesh strainer (BD Biosciences) and transferred in 5 ml FACs tubes for sorting. HUVECs expressing a high level of GFP were sorted and isolated using FACS Aria IIu Sorter with a 488nm laser at the Ross Research Flow Cytometry Core Facility (Johns Hopkins University School of Medicine, Baltimore, MD).

NuFF ECM experiments

Before NuFFs were seeded, coverglass Nunc Labtek Chamberslides were coated with 5ug/well human fibronectin (Sigma) for 1 hour at 37°C, 5% CO_2 in a humidified atmosphere. After the 1-hour incubation, the wells were washed three times with 1xPBS. NuFF (passages 20-28) cells were seeded at a cell density of $1.38x10^5$ cells/ml in each well and NuFF medium was exchanged every 2-3 days. The cells were cultured for 7 days at 37°C, 5% CO_2 in a humidified atmosphere before matrix de-cellularization.

Co-culture experiments

Before NuFF/MDA seeding, coverglass Nunc Labtek Chamberslides were coated with 5ug/well human fibronectin (Sigma) for 1 hour at 37°C, 5% CO_2 in a humidified atmosphere. After the 1-hour incubation, the wells were washed three times with 1xPBS. MDA231 and NuFF (passages 20-28) cells were seeded at the same time at a 1:1 ratio in the chamber slides. The total cell density in each well was $1.38x10^5$ cells/ml and media was exchanged every 2-3 days. The medium used was a 1:1 volume ratio of NuFF and MDA231 medium. The co-cultures were maintained for 7 days at 37°C, 5% CO_2 in a humidified atmosphere before matrix de-cellularization [27].

ECM de-cellularization and GFP-HUVEC seeding

The ECM was de-cellularized for 3-5 minutes using a 50nM NH_4OH buffer with 2% Triton X, lysing the cells while leaving the ECM behind. The de-cellularized ECM was washed three times with 1xPBS. Following this step, the ECM was incubated for 1 hour at 37°C, 5% CO_2 in a humidified atmosphere with 200 U/ml DNase I recombinant (RNase free) (Roche Scientific, Indianapolis, IN) to completely remove genomic DNA and all remaining cells. After this 1-hour incubation, the ECM was washed three times with 1xPBS and seeded with $2.0x10^5$ GFP-HUVECs [26, 27]. The chambers were cultured in HUVEC medium at above incubation conditions for 7 hours prior to live cell imaging.

Inhibition of fibronectin polymerization

Two peptides were used in the co-culture of NuFF and MDA231 cells to study the effects of fibronectin polymerization in the ECM on vascular formation: pUR4B and the control III-11C, which were a kind gift from Dr. Jane Sottile at Rochester University. They were obtained from cloning into Escherichia Coli and isolated as described by Chiang, H.Y., et al [35, 44]. The co-cultures were incubated in 250nM of pUR4B or III-11C [43]. The peptides were added 24 hours after NuFF/MDA231 seeding, and every day after for a total of 5 days.

Time-lapse imaging of GFP-HUVECs on ECM

Live cell time-lapse images were taken from hour 7 to hour 12 after GFP-HUVEC seeding on ECM using a Zeiss LSM 510 Meta Confocor 3 at the Integrated Imaging

Center (Johns Hopkins University, Baltimore, MD). Fluorescent z-stack images of step size 2-3um were taken with a 20x objective (Zeiss) every 15 minutes for 5 hours. An argon (488nm) laser was used to obtain the fluorescent images. Multi-Time 4.0.31 (Zeiss) was used to set up the time-lapse and Zen (Zeiss) was used to set up the image configurations. During the live cell time-lapse imaging the cells were cultured and incubated using conditions mentioned previously.

Immunofluorescence staining

After the live cell time-lapse imaging ceased (12 hours after GFP-HUVECs seeding) the cells were fixed with 3.7% paraformaldehyde for 30 minutes followed by a 10 minute incubation with 0.1% Triton X, which permeabilized the cells. After permeabilization, the cells were washed three times in 1xPBS and blocked with 1% bovine serum albumin (BSA) for 30 minutes. The samples were washed three times in 1xPBS and incubated with phalloidin546 (1:250, Molecular Probes) for an hour followed by another wash with 1xPBS. The samples were then incubated in DAPI (Dako) for 10 minutes followed by another wash with 1xPBS. One ml of 1xPBS was added to each well and stored at 4°C until imaged.

Confocal microscopy

Confocal images were taken with Zeiss LSM 510 Meta Confocor 3 with z-stacks of step size 0.7um to evaluate the morphology of the HUVECs and the presence of a lumen. The lasers used were Argon 488nm (GFP), He Ne 543nm (Phalloidin), and Chameleon Ti-Saphire tuned to 805nm (DAPI). Images were acquired using a 40X water objective.

Particle tracking

GFP-HUVEC cell migration was tracked using the Manual Tracking plugin (Fabrice P. Cordières, Institut Curie, France) in ImageJ (NIH). The x/y calibration was set to 0.877 um/pixel to covert pixels to microns and the time interval was set to 15 minutes. The center of the cell was used as a reference point for each cell in each frame. Cells that entered or exited the field of view during the 5-hour tracking time interval were excluded. Cells that underwent apoptosis or proliferation were also disregarded during the tracking process. Between 60 and 100 cells were tracked per condition per experiment. Each experiment was repeated three times and each condition was in duplicate. As stated before, the time interval was 15 minutes for a total of 5 hours.

Cell migration parameters

The cell migration parameters were calculated using a custom Matlab (The Mathworks, Natick, MA) code. The XY coordinates and the distance of each particle per frame retrieved by Manual Tracking were imported into Matlab. The migration parameters calculated were total distance travelled (of 5 hours), velocity between each frame, average velocity (of 5 hours), total displacement (of 5 hours), and mean square displacement. The total distance travelled per cell was calculated by summing the interval distances,

$$D_{total} = \sum_{i=1}^{N} D_i$$

Where D_{total} represents the total distance travelled, N is the number of distances, i represents each individual frame, and D_i is the distance travelled for each frame.

The velocity was calculated by dividing the interval distances by the interval time of 15 minutes,

$$V_i = \frac{D_i}{\Delta t}$$

where V_i is the interval velocity, and Δt represents the time interval (15 minutes). The following equation was used to calculate the average velocity,

$$V_{avg} = \frac{1}{N}\sum_{i=1}^{N} V_i$$

where V_{avg} represents the average velocity and N represents the number of total velocities. The total displacement was calculated using the following equation,

$$d_{net} = \sqrt{\left(x_f - x_i\right)^2 + \left(y_f - y_i\right)^2}$$

where d_{net} represents the net displacement of a cell, x_f is the final x position, x_i is the initial x position, y_f is the final y position, and y_i is the initial y position. Mean square displacement is a parameter often used to characterize the motility of cells along with the previously mentioned parameters. It was calculated using the following equation,

$$MSD = \left\langle \left[r\left(t+\tau\right) - r\left(t\right) \right]^2 \right\rangle$$

where MSD presents the mean square displacement, r(t) is the position of the particle at time t, τ is the lag time between the two positions.

Statistical Analysis

The statistical analysis was performed using GraphPad Prism 6.0 (GraphPad Software Inc., La Jolla, CA). The One Way ANOVA with multiple comparisons and Turkey's posttest was used to analyze the significance. All graphs are displayed with mean±SEM

unless otherwise stated. The significance was measured at *$p \leq 0.05$, p**≤ 0.01, p***≤ 0.001. All experiments were repeated three times with each condition in duplicates.

Results

A series of experimental steps were taken to determine the effect of the fibronectin network on endothelial cell migration. **Figure 3** illustrates the various steps taken to determine the effect.

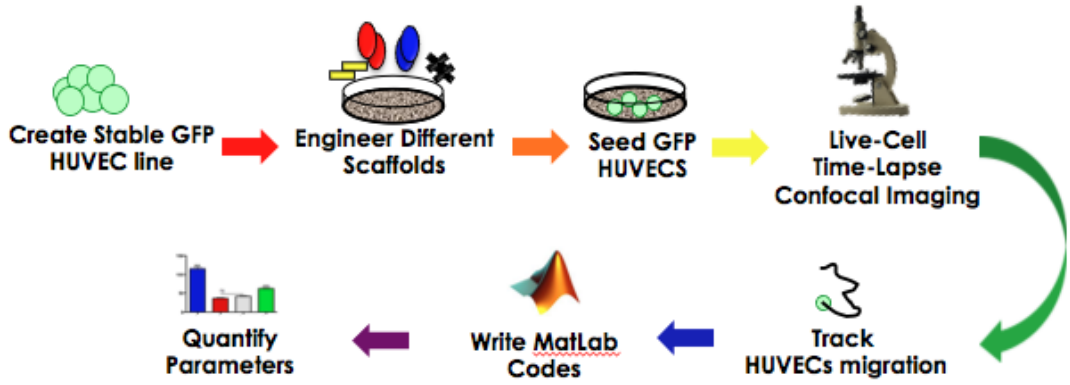

Figure 3: Outline of Experimental Steps. The figure above illustrates the series of experimental steps taken to determine the effect of a fibronectin network on endothelial cell migration.

Cell lines and culture

Three cell lines were used in the following experiments: human umbilical cord vein endothelial cells (HUVECs), human breast cancer cells (MDA231), and neonatal foreskin fibroblasts (NuFFs). The cells were cultured and passed as previously described. As shown in **Figure 4,** each cell has its own distinct morphology. The HUVECs maintained a cobblestone like pattern upon reaching confluency. Once they reach the point of over confluency they become round and start to detach from the surface. MDA231 cells had a more rod like morphology while NuFFs maintained a stretched and elongated shape in cell culture. A light microscope was used to visualize the morphology of all cells to ensure they were alive and healthy throughout the experiments.

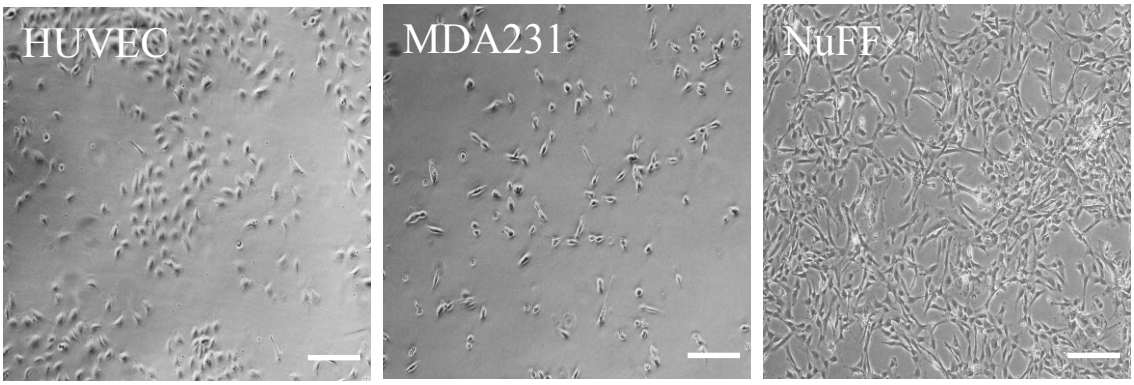

Figure 4: Phase Contrast Images of Cells in Culture**.** These phase contrast images represent the different cell lines used in the experiments. Each line has its own distinct morphology. Scale bars = 100μm.

GFP transfection and cell sorting

Before beginning the endothelial cell migration experiments, HUVECs were transfected with a green fluorescent protein (GFP) using lentiviral GFP. This was a stable transfection and allowed the HUVECs to emit green fluorescent light at an emission of 488nm using a fluorescent microscope. These fluorescently tagged cells would eventually allow the cells to be tracked during their migration and create clear, concise fluorescent images to optimize the tracking process.

After the transfection was completed, the cells were sorted according to their fluorescent intensities. **Figure 5** shows the gates used to sort the GFP-HUVEC population.

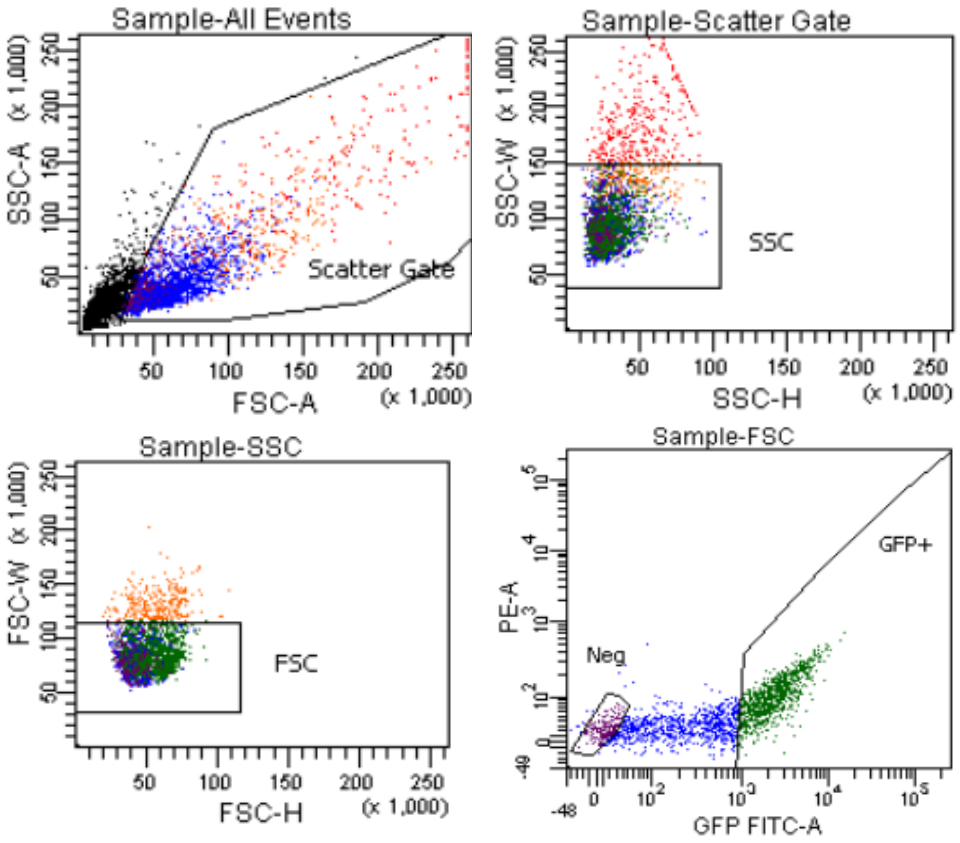

Figure 5: GFP HUVEC Sorting. These plots present the different stages of sorting the GFP transfected HUVECs into three subpopulations: GFP Negative, GFP Low, and GFP High.

After narrowing the population of cells using side scattering (SSC) and forward scattering (FSC), 3 subpopulations were created: GFP Negative, GFP Low, and GFP High. The Sample-FSC plot shows the 3 subpopulations. The purple data points represent the GFP Negative cells, the blue data points represents the GFP Low cells, and the green data points represent the GFP High cells.

After the GFP transfected HUVECs were sorted into the 3 subpopulations, images were taken to ensure their fluorescent intensities were representative of the sorting results. **Figure 6** displays phase contrast and fluorescent images of GFP High, GFP Low, and GFP Negative HUVECs.

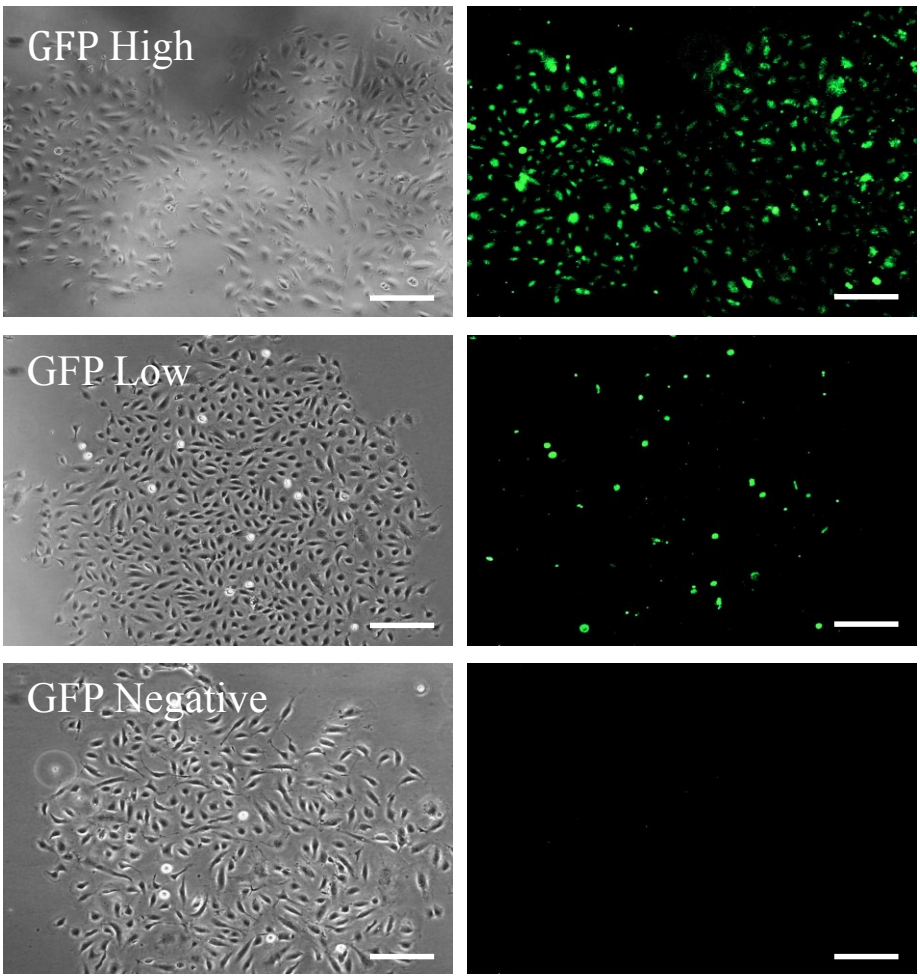

Figure 6: GFP High, GFP Low, and GFP Negative HUVECs. Above are phase contrast and fluorescent images of the three subpopulations. Scale bars =100μm.

It is evident that the fluorescent intensity is highest in the GFP High subpopulation. There is some green fluorescence present in the GFP Low subpopulation, but it is not as intense as the GFP High HUVECS. In addition, it is clear that there is no fluorescence present in the GFP Negative HUVEC subpopulation. To optimize the live cell time-lapse experiments, GFP High HUVECs were used for all experiments. The

extent of fluorescence in this subpopulation decreases the necessary exposure and further prevents the cells from photo bleaching during the 5 hour imagine time period.

Determining an optimal concentration of inhibitor and control peptide

After sorting the GFP transfected HUVECs and verifying the subpopulations high fluorescence intensity, an optimal dose of the fibronectin inhibitor pUR4B and the control peptide III-11C were determined to use in the NuFF/MDA231 co-culture experiments. While a concentration of 250nM for both the inhibitor and control was used in previous studies, we sought to verify that this specific concentration worked for our experiments [43].

To determine the effect of pUR4B on fibronectin polymerization within the ECM, the inhibitor was added to the culture daily. After 4 days of culture, the cells and scaffold were fixed and stained for fibronectin. Three different concentrations of the inhibitor were used to determine the best dose to use for our experiments: 250nM, 375nM, and 500nM. **Figure 7** shows the results of this test.

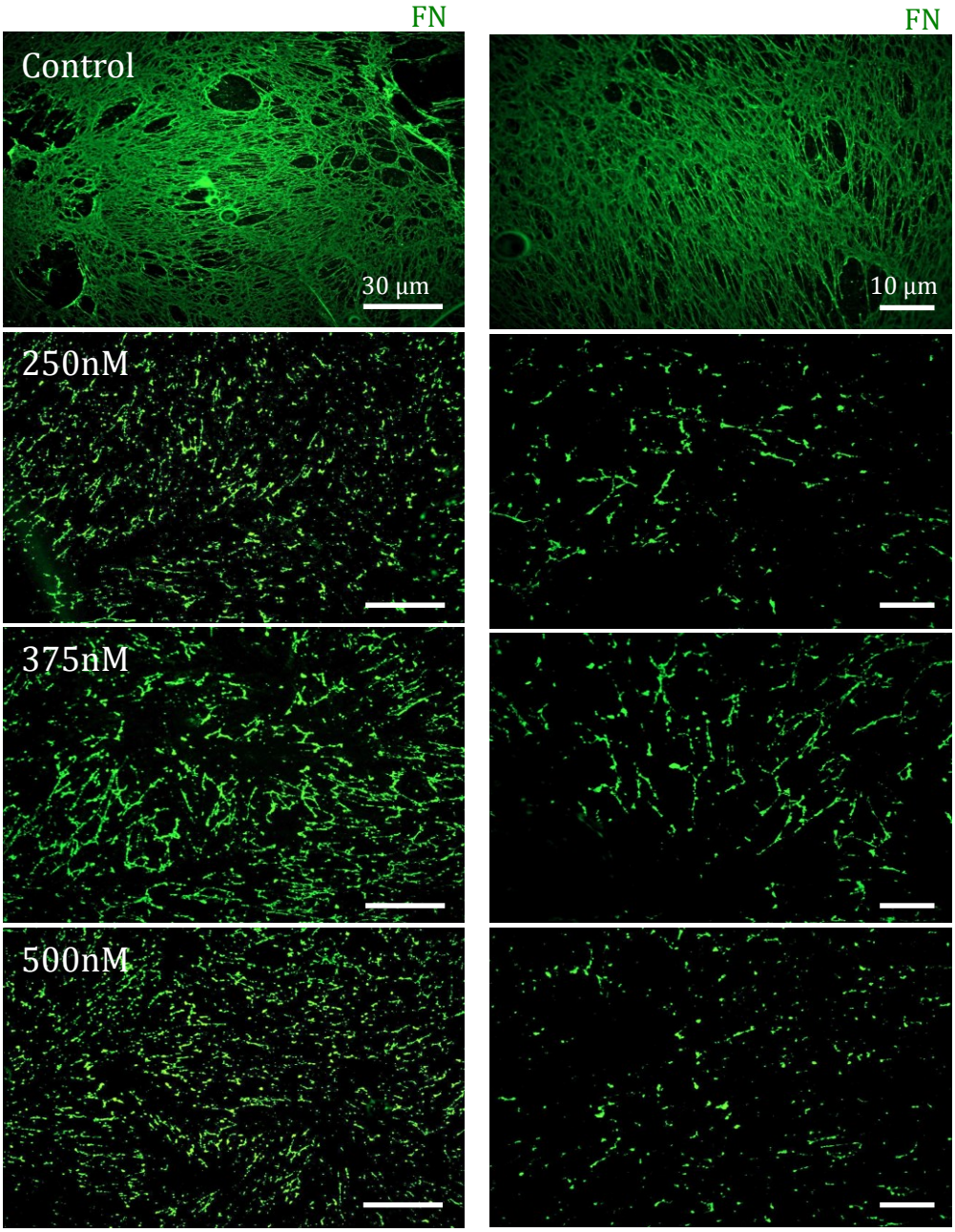

Figure 7: pUR4B test on Fibronectin Polymerization. The fluorescent images above show the effect of various concentrations of pUR4B, the fibronectin polymerization inhibitor on NuFF derived ECM. The control is without the addition of the inhibitor. The scale bars on the left column of images represent 30µm and those on the right column represent 10µm.

It is clear that fibronectin is present in a polymerized network without the addition of the inhibitor. The inhibitor prevented fibronectin polymerization to a significant degree in all concentrations used. It is evident that the fibronectin protein is still present in the ECM, displayed by the sparse fluorescent fibrils in the images, but the network formation as seen in the control is not present. As the concentration of the inhibitor increases, the degree of unpolymerized fibronectin does not increase. Therefore, experiments were followed through with the previously tested concentration of 250nM.

Scaffold preparation

Three different scaffolds were used to study the cell migration of the GFP High HUVECs during vascular morphogenesis. In addition, the migration of GFP High HUVECs on a bare coverglass chamber was used to compare the migration parameters in the absence of any ECM components. Scaffold preparation consisted of a 7-day culture period of the NuFF, MDA231 cells, and the inhibitor or control peptide. During the 7-day culture period, the cells deposited copious amounts of ECM proteins. After the 7 days, the cells were overly confluent and ready to by lysed and removed from the protein rich scaffold. **Figure 8** displays phase contrast images of the three cell culture conditions prior to de-cellularization.

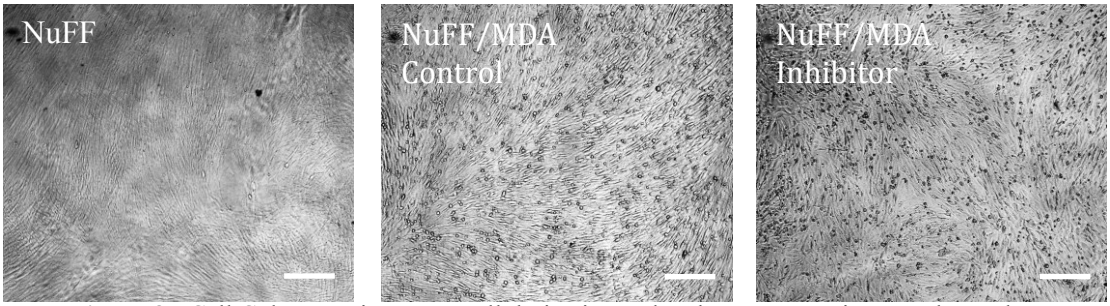

Figure 8: Cell Cultures Prior to De-cellularization. The phase contrast images above show the three different protein rich scaffolds prior to de-cellularization. Scale bars = 100μm.

The following describes the three scaffold conditions shown in the figure above: NuFF cells alone, a co-culture of NuFF and MDA231 cells with the daily addition of 250nM the control peptide III-11C, and a co-culture of NuFF and MDA231 cells with the daily addition of 250nM of fibronectin polymerization inhibitor pUR4B. The co-culture scaffolds were used to mimic a breast cancer ECM, while the NuFF derived ECM was used to compare with the breast cancer model. The first image shows over confluent NuFFs. Their morphology was extremely elongated and they were aligned in the same direction. The next image shows the NuFF and MDA231 cells in co-culture with the control peptide. The elongated cells are NuFFs and the more rounded cells are MDA231. The third image is of NuFF and MDA231 cells with the addition of pUR4B. Similar to the breast cancer ECM with the control peptide, the elongated cells are NuFFs and the MDA231 cells are those with the rounded morphology. The NuFF alignment in the co-culture with the control resembles that of the condition with NuFFs only. The NuFF alignment of the co-culture with the inhibitor looks to be more random than that of the other two conditions.

HUVEC seeding and endothelial cell tracking

After the cells were lysed and removed, GFP High HUVECs were seeded on top of the de-cellularized matrices from each of the above tested conditions at hour 0. The GFP High HUVECs were seeded on a bare coverglass chamber as a control. Live cell time-lapse images were taken at 15-minute intervals for 5 hours, beginning at hour 7 post seeding and ending at hour 12 post seeding. These time-lapse images were used to track the migration of the HUVECs. The Manual Tracking plugin on ImageJ was used to

obtain the coordinates of the positions of the cells at each time point. The center of the cells was used as a reference point for each frame. **Figure 9** shows the GFP High HUVECs trajectories in each condition for the 5 hour time period in 1-hour intervals.

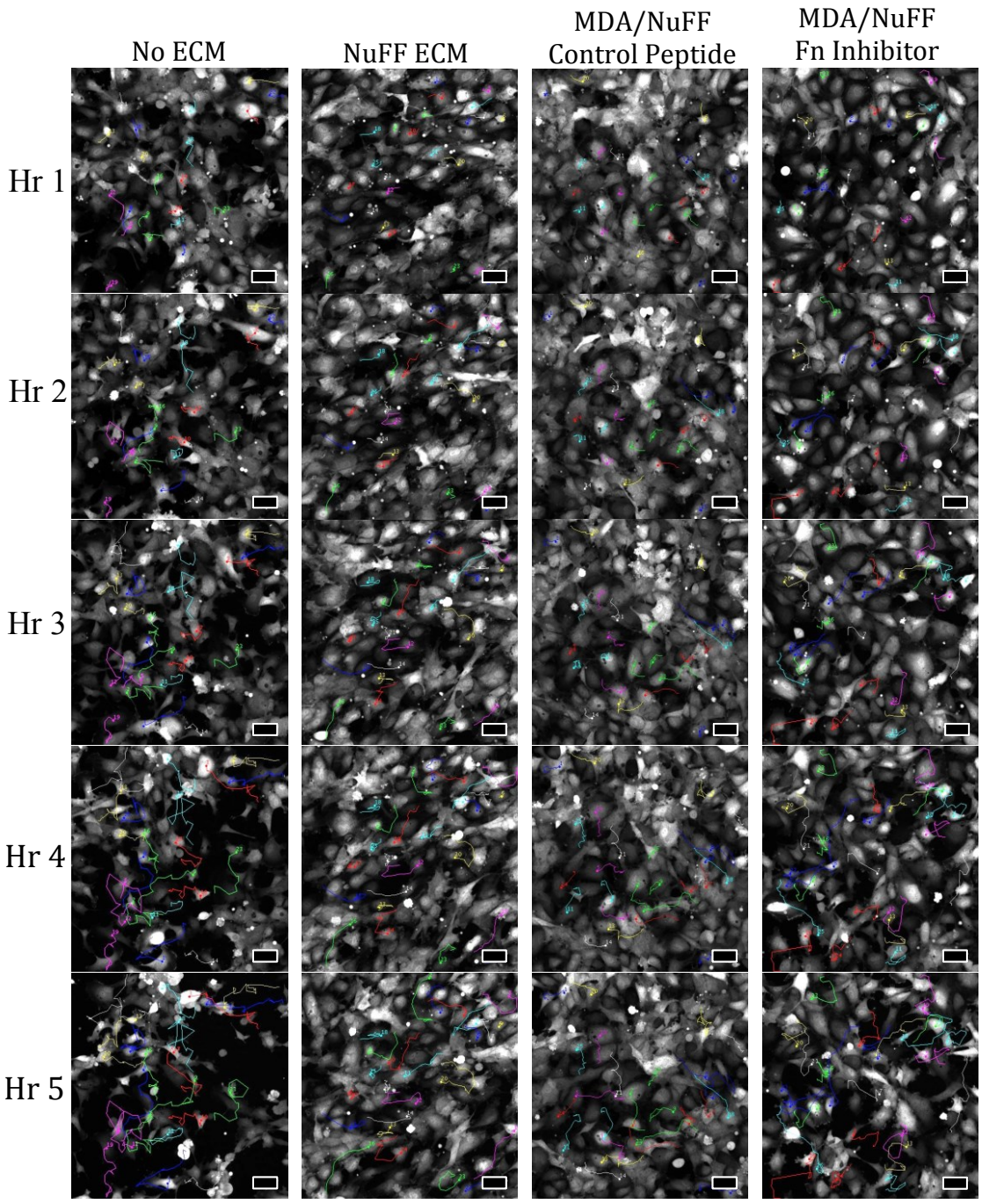

Figure 9: Cell Tracking Trajectories. The images above display the trajectories of the GFP High HUVECs on each scaffold. The scale bars represent 50 μm.

The images in **Figure 9** are grey scale to make the cell trajectories more visible. Each column represents a scaffold condition used: no ECM, NuFF ECM, MDA/NuFF with the control peptide, and MDA/NuFF with the inhibitor. The Hour 1 images are the trajectories of the cells after 1 hour, corresponding to the 8^{th} hour after seeding. The colored lines represent the GFP High HUVECs trajectories, and the colored dots attached to the lines represent cells' positions at the designated time. The trajectories at the 5-hour time point show the path of the cells at the end of the experiment, representing the cells' total distance travelled.

Endothelial cell migration quantification

In order to quantify the total distance travelled by the cells, and the other migration parameters mentioned earlier, the data was exported from Manual Tracking (Fabrice P. Cordières) into Matlab (Mathworks). Custom codes were used to generate the migration parameters. The total distance travelled by the GFP High HUVECs during the 5-hour time-lapse imaging was first calculated and compared among the four scaffold conditions. **Figure 10** shows the results of the total distance travelled.

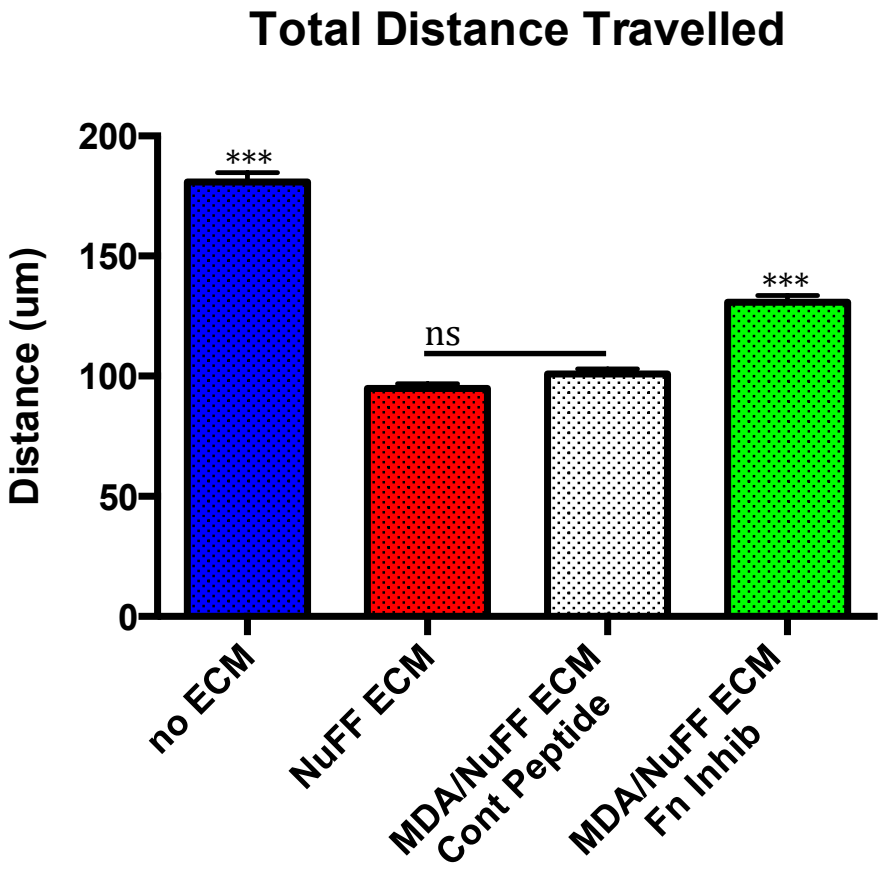

Figure 10: Total Distance Travelled. This graphs shows the mean total distance travelled by the GFP High HUVECs in each scaffold condition. Note that *** represents significance with all other conditions with $p \leq 0.001$. "ns" corresponds to no significance. The error bars represent the standard error of mean.

The total distance travelled was measured in microns and each column represents a different scaffold condition. It is evident that the HUVECs seeded in the absence of an ECM travelled the largest distance with a mean value of 180.9µm. This distance was statistically significant compared to the other three conditions ($p \leq 0.001$). The GFP High HUVECs travelled the second largest distance in the breast cancer ECM with the inhibitor. With a mean value of 130.8 µm this was also significantly different compared to the other three conditions ($p \leq 0.001$). The total distances travelled by the HUVECs on

the NuFF ECM and breast cancer ECM with the control peptide were similar with mean values of 94.9 μm and 100.9 μm, respectively. While these two values were significantly different compared to that of no ECM and the breast cancer ECM with the inhibitor, there was no significant difference between the two.

In addition to total distance travelled, we also calculated the net displacement of the GFP High HUVECs on each scaffold from 7 to 12 hours post seeding. **Figure 11** displays the results of net displacement.

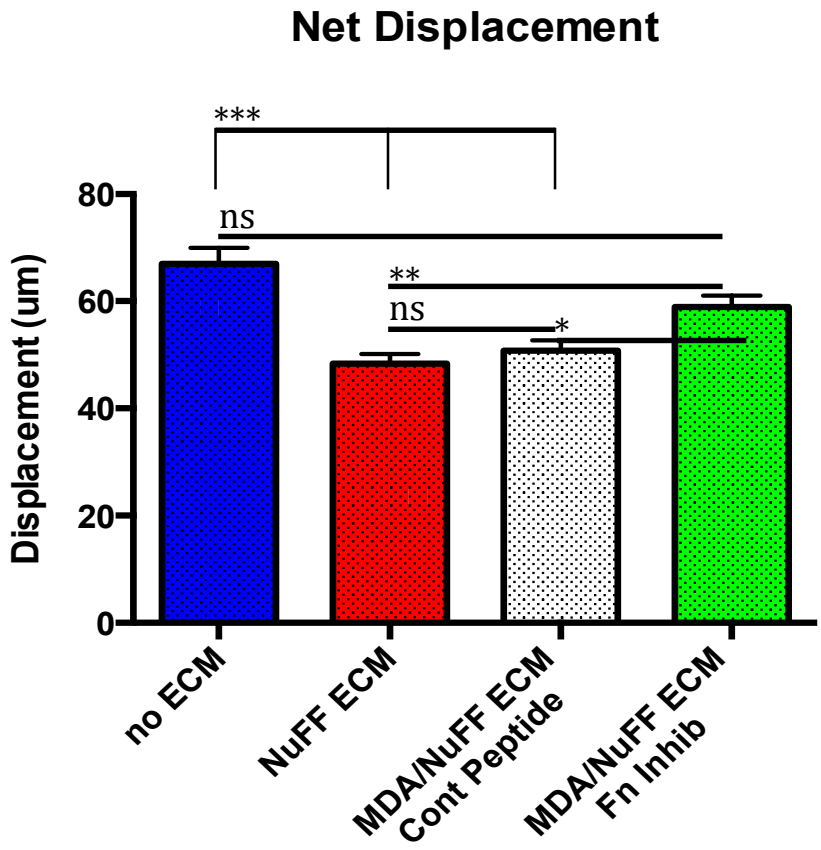

Figure 11: Net Displacement. This graph displays the net displacement for the 5-hour time period of the GFP High HUVECs for each scaffold condition. Significance is measured as *** $p \leq 0.001$, ** $p \leq 0.01$, * $p \leq 0.05$. The error bars correspond to the standard error of mean.

Net displacement was measured in microns and each column represents a different scaffold condition. HUVEC net displacement was largest in the absence of an ECM with a mean value of 67.00 μm, which was significantly different than the net displacement of HUVECS on both the NuFF ECM and the breast cancer ECM with the control peptide ($p \leq 0.001$). However, it was not significant compared to the net displacement of HUVECs on the breast cancer ECM with the inhibitor, which had a mean value of 58.93μm. The net displacement of HUVECs on breast cancer ECM with the inhibitor was significantly different compared to that on NuFF ECM ($p \leq 0.01$) and breast cancer ECM with the inhibitor ($p \leq 0.05$). The HUVECs on the NuFF ECM and the breast cancer ECM with the control peptide had net displacements of 48.39μm and 50.79μm, respectively, and were not significantly different from each other.

Another migration parameter we quantified was the average velocity of the HUVECs on each scaffold. This parameter provided an understanding of HUVECs rate of migration. **Figure 12** shows the average velocity of the GFP High HUVECs on each scaffold condition for 7 to 12 hours post seeding.

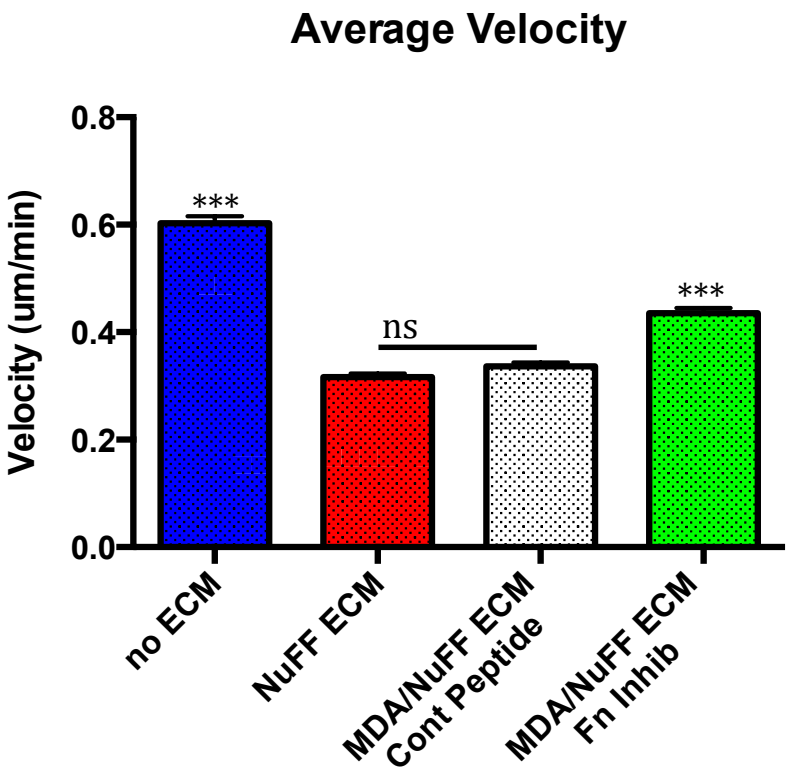

Figure 12: Average Velocity. The graph above shows the mean average velocity of the GFP High HUVECs for each of the 4 scaffold conditions. The error bars represent the standard error of mean. *** P≤0.001 and "ns" corresponds to no statistical difference.

The average velocity was measured in μm/min and each column represents a different scaffold condition. The GFP High HUVECs migrated at the highest rate in the absence of an ECM with a value of 0.603 μm/min. The second highest velocity was 0.436 μm/min and occurred in the breast cancer ECM with the addition of the inhibitor. Both of these velocities were significantly different compared to each other as well as the other two conditions ($p \leq 0.001$). The two lowest velocities were 0.336 μm/min and 0.316 μm/min, which occurred in in breast cancer ECM with the control peptide and the NuFF ECM, respectively. Each of the lowest average velocities was significantly different

compared to the highest rates ($p \leq 0.001$), but showed no significance compared to each other.

In addition to average velocity, we calculated the interval velocities at each 15-minute time interval for the 5-hour duration. **Figure 13** shows the HUVEC velocities for each scaffold.

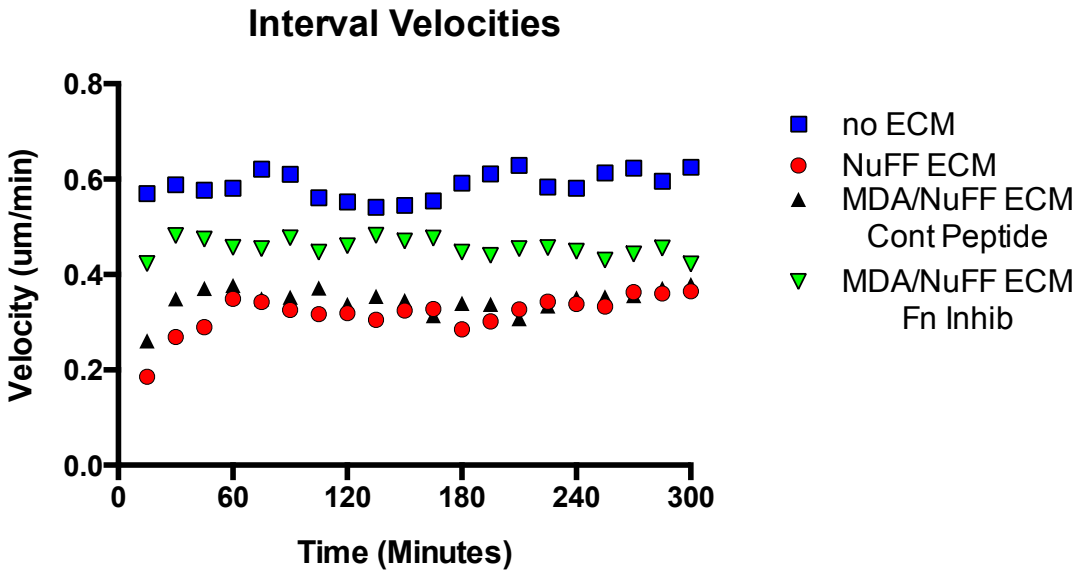

Figure 13: Interval Velocities: This graph displays the HUVECs' velocities at each 15 minute interval time point for five hours as a function of time. The velocities of the HUVECs in each scaffold each represented by a different color and shape. Note that the error bars are not included in the graph to optimize the clarity of the graph.

The interval velocities were measured in μm/min and each colored symbol represents a different scaffold condition. The time scale goes from 0 to 300 minutes; t=0 corresponds to hour 7 after the GFP High HUVECs were seeded onto the scaffolds and t=300 minutes corresponds to hour 12 after seeding. Similar to the previous graphs, the HUVECs that were cultured in the absence of an ECM had the highest velocities through out the 5-hour period. There is no linear trend that the cells seem to follow without an

ECM. The cells stay at a constant velocity of about 0.6 um/min, which is consistent to the average velocity shown in **Figure 12**. The HUVECs on the breast cancer ECM with the inhibitor also remains as a constant velocity around 0.45 μm/min. In fact the velocities in all conditions remain constant through the 5-hour time period except for the NuFF ECM and the breast cancer ECM with the control peptide for the first hour. These velocities increase linearly until they reach the 1-hour mark and then remain at a constant rate of about 0.3μm/min. While the velocities in the breast cancer ECM with the inhibitor and that in the absence of an ECM don't overlap with any other data points, the velocities in the other two conditions overlap many times through the 5-hour period. This is consistent with the other cell migration parameters calculated.

The last cell migration parameter that was quantified was the mean square displacement (MSD) of the GFP High HUVECs on each scaffold condition. This parameter gives us an understanding of the dynamics of the HUVECs and relates to the mechanical properties of each scaffold. **Figure 14** shows the graph of MSD for each scaffold condition from 7 to 12 hours post GFP High HUVEC seeding.

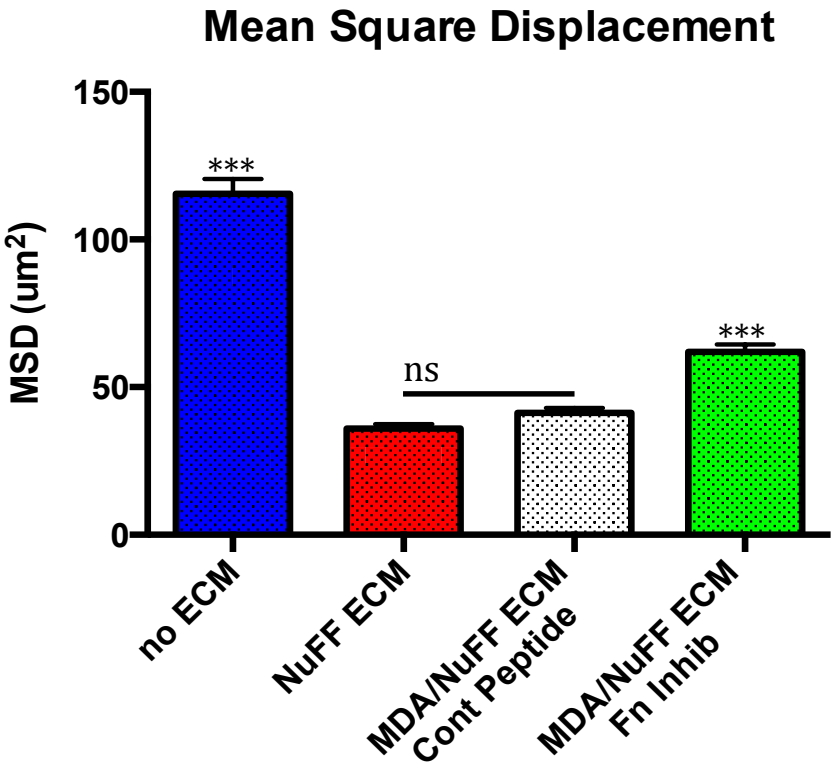

Figure 14: Mean Square Displacement. The graph above displays the mean square displacement of GFP High HUVECs for each scaffold condition. The error bars represent the standard error of mean. *** P≤0.001 and "ns" corresponds to no statistical difference.

Each column in the graph represents a different scaffold condition. The MSD of the GFP High HUVECs was the largest in the absence of an ECM with a value of 115.5 μm^2, which was significantly different than the MSD of the other three conditions ($p \leq 0.001$). The second largest MSD was that of the breast cancer ECM with the inhibitor with a value of 61.91 μm^2, which also proved to be significantly different than all other conditions. The MSD of the HUVECs in the NuFF ECM and breast cancer ECM with the control peptide were 35.90 μm^2 and 41.34 μm^2, respectively. While these were

significantly different than the MSD in the other two conditions, there was no significance between the two.

Fluorescent imaging of HUVECs after 12 hours post seeding

After imaging the live GFP High HUVECs from hour 7 to hour 12 post seeding, we fixed and stained the cells for phalloidin and DAPI. We used fluorescent confocal imaging to visualize the morphology of the HUVECs on each of the scaffold. Z-stacks were taken with a slice interval of 0.7 μm. **Figure 15** shows the fluorescent images of the HUVECs morphology.

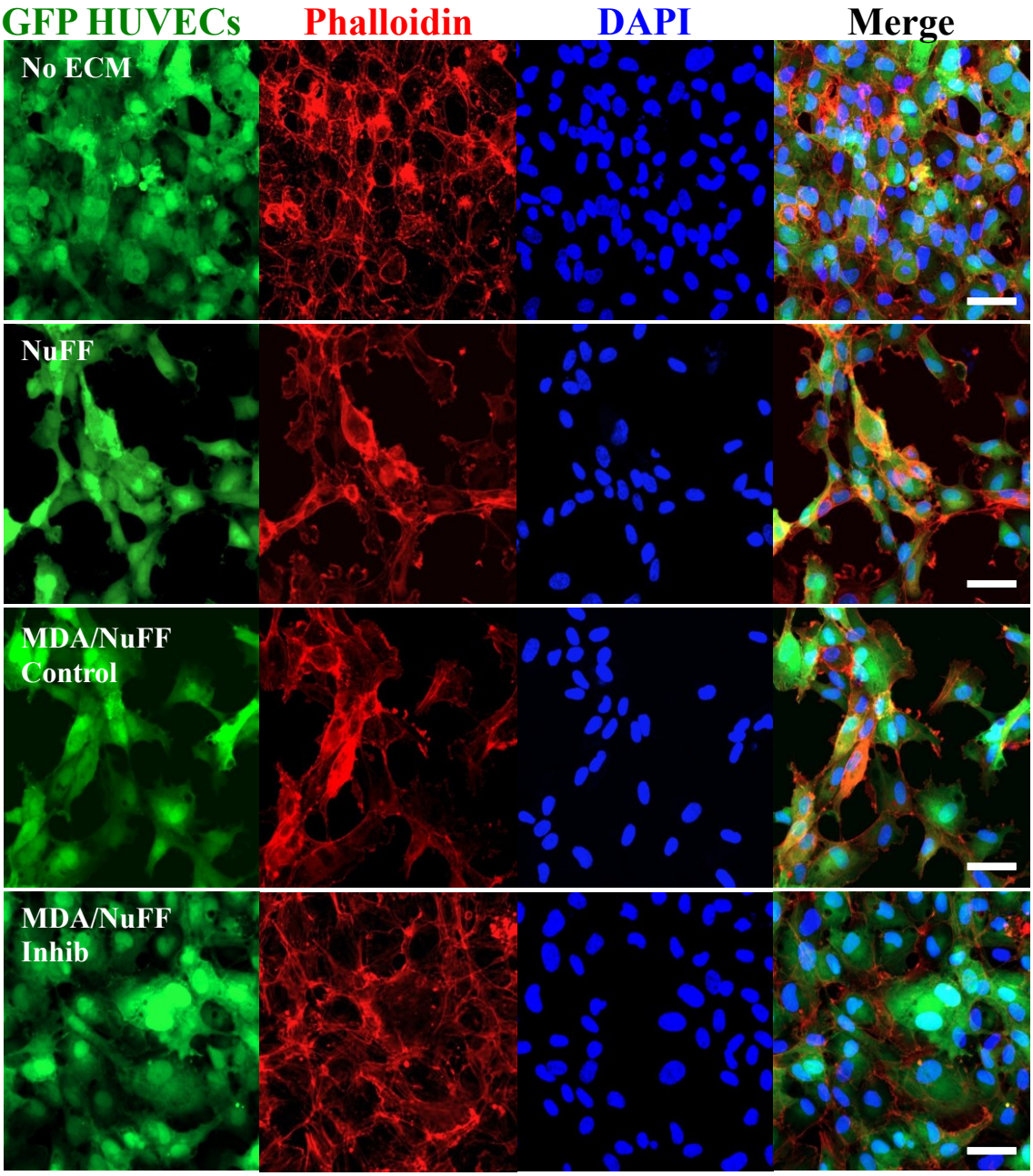

Figure 15: Fluorescent Images of HUVECs 12 Hours Post Seeding. The images above display the morphologies of HUVECs for each scaffold condition. The green images represent the GFP High HUVECs, the red corresponds to phalloidin, and the blue corresponds to DAPI. The images in the fourth column represent the merged image. The scale bars measure 100μm.

Each row corresponds to a different scaffold condition, while the rows represent the GFP HUVECs, phalloidin, DAPI, or a merge of all three. Phalloidin binds to F-actin, showing the cytoskeleton of the cells, and DAPI binds to the nucleus. The cells in the first row, corresponding to the HUVECs seeded in absence of an ECM, show no evidence of vascular organization. The positions of their nuclei are not arranged in any organized pattern nor do they align to form any capillary like structures. However, in the second row, displaying cells in the NuFF derived ECM, it is evident that there is some organization among the cells. The GFP and phalloidin images show some organization of the HUVECs and the cells' cytoskeleton. The DAPI also shows alignment of the nuclei along the organization consistent with the phalloidin and GFP images. It is also clear that organization of the HUVECs exists on the MDA/NuFF ECM with the control peptide. The GFP and phalloidin images show structure like formations that are consistent with each other. The DAPI image also shows some alignment of the nuclei, matching up with the microvascular like structures of the GFP and phalloidin images. Like the No ECM control, the MDA/NuFF ECM with the inhibitor shows no distinct arrangement or organization. There are no capillary like structures, and the DAPI image does not show any nuclei alignment.

Discussion

The ECM is a protein-rich entity composed of several constituents that are capable of translating signals to regulate cell behaviors such as adhesion, migration, proliferation, differentiation, and survival. Some of the most studied components are laminin, collagens I and IV, elastin, and fibronectin, and each of these can serve its own distinct function within the ECM. While all the components are crucial to regulating cell behavior, we focused on studying the unique function of a cell-derived polymerized fibronectin matrix on endothelial cell migration. Here we used two fibroblast-derived ECM's to mimic the native physiological and structural microenvironment found in vivo: a NuFF-derived ECM and a NuFF-derived ECM that was co-cultured with a breast cancer cell line MDA231. The co-culture ECM was used to mimic the microenvironment of a breast cancer tumor, while the NuFF-derived ECM was used to mimic normal, non-tumorigenic ECM. In order to study the unique function of fibronectin in its natural polymerized state within the ECM, we used pUR4B, a peptide that inhibits the polymerization of fibronectin. We also used III-11C, a peptide that has no effect on fibronectin polymerization as a control to determine pUR4B's effects on endothelial cell migration.

The results presented on the different migration parameters on each of the scaffold conditions demonstrate that fibronectin does play a key role in endothelial cell migration. More specifically, the network in which fibronectin forms, plays a large role in the migration of endothelial cells. To recall, the four scaffold conditions used were: a bare coverglass bottom chamber denoted as no ECM; a NuFF-derived ECM; a co-culture of NuFF and MDA231 ECM with the addition of III-11C, the control peptide; and a co-

culture of NuFF and MDA231 ECM with the addition of pUR4B, the fibronectin polymerization inhibitor. The goal was to determine the effect of polymerized fibronectin on endothelial cells' migratory behavior. Cell migration is regulated by many ECM components, so the no ECM scaffold gives us an understanding of the migration without any of the physiological cues or structural architecture relative to the native nature of the ECM. Our hypothesis was that polymerized fibronectin would significantly influence endothelial cell migration during the angiogenic cascade, as it was discovered to inhibit angiogenesis [35, 43].

The first cell migration parameter quantified was the total distance travelled by the HUVECs in each scaffold condition. **Figure 9** shows the cells' trajectories over the 5-hour imaging experiment. These trajectories at the 5-hour mark represent the total distance travelled by the cells during the imaging period. It was difficult to draw any conclusions from the trajectories themselves; therefore the distances were quantified as can be seen in **Figure 10**. These total distances travelled by the HUVECs varied with each scaffold condition. It was highest in the absence of an ECM with a value of 180.9 μm. This distance was extremely high compared to the distance of the other scaffolds tested as the components of the ECM were not present to restrict migration or act as an adherent structure. The total distance travelled by the HUVECs seeded on the NuFF ECM was much lower than that seeded in the absence of the ECM. This was due to the presence of the various components of the fibroblast-derived ECM. The different constituents of the ECM provided the HUVECs with a structural scaffold and binding sites to adhere to. The HUVECs on the breast cancer ECM with the addition of the control peptide showed a similar total distance travelled to that on the NuFF ECM. There

was no statistical significance between the two, allowing one to assume these two scaffolds were comparable. The smaller distance travelled was also due to the varying ECM components present including polymerized fibronectin, allowing for cell adhesion, which contributed to restricted cell migration. A notable result was the total distance travelled by HUVECs on the breast cancer ECM with the addition of pUR4B. The mean total distance travelled was 130.8 μm and proved to be significantly different than all other conditions. There are many factors that contribute to the difference. Firstly, the components of the ECM are present allowing the HUVECs to adhere, which explains why the distance is much smaller than that of no ECM. However, the distance was much larger than it was on the NuFF and control breast cancer ECM, and this difference was due to the inhibitor. This shows that polymerized fibronectin significantly restricts endothelial cell migration in a breast cancer ECM model. In the presence of polymerized fibronectin, HUVECs showed a much smaller path. This indicates that fibronectin in its polymerized network provides a more adherent scaffold within the ECM than unpolymerized fibronectin. In addition to these significant findings, other quantified migration parameters also demonstrated the restricting effects of polymerized fibronectin in the ECM on HUVECs during angiogenesis.

The net displacement of HUVECs on each scaffold condition also showed that polymerized fibronectin plays a role in endothelial cell migration during angiogenesis. Net displacement is the measurement of the distance from a cell's position at t=0 to t=300 minutes and allows us to see how far the cell travelled from its original position. Unlike the total distant travelled, this parameter only takes into consideration the first and last position whereas the total distance travelled incorporates all distances travelled by a cell

from t=0 to t=300 minutes. Similar to total distance travelled, HUVECs in the absence of an ECM had the largest displacement with a value of 67.0 μm. The second largest net displacement of HUVECs occurred in the breast cancer ECM with the inhibitor with a value of 58.93 μm. The difference between these two net displacements can be explained by the presence of the ECM constituents. The breast cancer ECM incorporates the many native ECM components allowing the HUVECs to adhere, ultimately impeding migration from their initial position. However, with the addition of the inhibitor, fibronectin is not in its polymerized network. When fibronectin is present in its polymerized network within the ECM, the net displacement decreases to 48.39 μm (NuFF ECM) and 50.79 (breast cancer ECM with control peptide). When fibronectin is present in its polymerized network, it seems to provide the HUVECs with a more adherent scaffold, retarding the migration from the cells' original starting positions at t=0.

In addition to total distance travelled and net displacement, the average and interval velocities of the HUVECs on each scaffold were quantified to gain an understanding of the effect polymerized fibronectin has on the rate at which endothelial cells migrate during angiogenesis. Once again we saw that the highest rate at which the HUVECs travelled was in the absence of an ECM. This is due to the lack of ECM components, and therefore no molecules to adhere, which resulted in a higher rate at which the cells migrate. While the average velocity of the HUVECs in the absence of no ECM was 0.603 μm/min, that of HUVECs on the breast cancer ECM with the inhibitor was significantly lower with a value of 0.436 μm/min. As mentioned earlier this lower cell velocity is due to the constituents of the ECM providing an adherent scaffold for the HUVECs and retarding the rate at which they migrate. The scaffolds incorporating a

polymerized network of fibronectin into the ECM retarded the migration rate even more with average velocities of 0.316 μm/min (NuFF ECM) and 0.336 μm/min (breast cancer ECM with control peptide). In addition to the average velocities, another way we analyzed the cell migration rates in response to the inhibitor was the interval velocities through out the 5-hour time period. As stated earlier, images were taken every 15 minutes for 5 hours. We calculated the velocities for each 15-minute interval to analyze the trends of the cells' velocities over time (**Figure 13**). The results were consistent with the average velocities calculated in **Figure 12**. There is a clear difference in velocities between the HUVECs on no ECM and HUVECs in the breast cancer ECM with the inhibitor. As stated before this difference is due to the adherent ECM components present in the breast cancer ECM. This graph also clearly shows the overlap in velocities of HUVECs in the NuFF ECM and the breast cancer ECM with the control peptide. The velocities are lower due to the presence of fibronectin in its polymerized network. In the presence of the inhibitor, the velocity of HUVECs is notably larger which is a result from the lack of polymerized fibronectin.

The mean square displacement (MSD), a commonly used parameter in cell migration studies, was the last parameter quantified in order to analyze the effect of the inhibitor on endothelial cell migration during angiogenesis. The MSD of HUVECs in the difference scaffold conditions also provided additional proof that the inhibitor has a significant effect on endothelial cell migration. The graph (**Figure 14**) shows results similar to the graphs of the other migration parameters. The MSD was largest when HUVECs were in the absence of an ECM and second largest in the breast cancer ECM with the inhibitor. The MSD's in both of these conditions were significantly different

compared to each other and the other two scaffolds. The MSD's of HUVECs in the NuFF ECM and the breast cancer ECM with the control peptide were both the lowest and were not significantly different from each other. The differences in the MSD's among the scaffolds can be accredited to the presence of ECM constituents, and more importantly a polymerized fibronectin network.

The results from our experiments proved that a polymerized fibronectin network in the ECM restricts endothelial cell migration during angiogenesis. The fluorescent images at the 12-hour time point post HUVEC seeding demonstrate that organization among the endothelial cells occurs with nuclei alignment into vascular like structures. A lumen was not present within the organized structures, but we predict that it forms at a later time point, as other researchers have reported evidence of vascular lumens 24 hours post endothelial cell seeding [26, 27]. Nevertheless, vascular organization occurred up to hour 12 post seeding in the two scaffolds in which fibronectin was polymerized. There was no evidence of microvasculature of HUVECs in the absence of an ECM and on the breast cancer ECM with the inhibitor.

The results from our work prove that the polymerized network of fibronectin has a significant effect of endothelial cell migration. While providing a supportive scaffold for the HUVECs, the polymerized fibronectin network in the ECM retards the rate at which they migrate. Not only does the fibronectin network provide a more adherent network for the endothelial cells it may also affect the organization of other ECM components further having an effect on cell migration. The results presented here are important for the field of angiogenesis and can contribute to a greater understanding of the role of polymerized fibronectin on endothelial cell migration. Such research may

serve as a platform for future studies investigating the use of fibronectin polymerization inhibitors as an anti-angiogenic cancer therapy.

Conclusion

Angiogenesis has been extensively studied due to its role in regenerative medicine, tissue engineering, and cancer development and growth. An entity identified to regulate angiogenesis is the microenvironment in which this process occurs, known as the ECM. As scientists are gaining a deeper understanding of the ECM, they are focusing on manipulating certain molecules within the scaffold to inhibit angiogenesis. One protein of interest known for its presence as a polymerized network in the ECM and role in angiogenesis is fibronectin. Our work aimed to study the effects of pUR4B, a peptide that inhibits the polymerization of fibronectin, on endothelial cell migration in a fibroblast derived ECM and fibroblast-breast cancer derived ECM.

By quantifying cell migration parameters such as total distance travelled, net displacement, cell velocity, and mean square displacement of HUVECs on the different scaffolds we found that the polymerized fibronectin network had a significant effect on endothelial cell migration. We observed that endothelial cells in the absence of an ECM travelled the farthest distance and at the highest rate. The endothelial cells that were seeded on a breast cancer ECM with the fibronectin polymerization inhibitor travelled the second largest distance at the second largest rate, while endothelial cells in the NuFF ECM and breast cancer ECM with the control peptide travelled the smallest distances and at the lowest rates. The difference in migration between the HUVECs in the breast cancer ECM's with the inhibitor and with the control peptide are due to the polymerized fibronectin network. The difference can be explained by the altered structural support within the ECM and the adherent traits of the polymerized fibronectin network. This altered ECM structure effects the migration and motility of endothelial cells.

Our findings are significant and provide a further understanding of endothelial cell migration in a manipulated ECM. They also confirm that fibronectin plays a crucial role in angiogenesis as its polymerized network alters the structure and adherent ability of the ECM. The work presented here has delivered insight into the effects of pUR4B on the ECM, and ultimately endothelial cell migration, and could potentially be used to study the role of additional molecules during angiogenesis.

Future Work

This work established significant findings on the effects of polymerized fibronectin in the ECM on endothelial cell migration, but further studies can be done to gain a more in depth understanding.

Firstly, in the future, I would propose to extend the time period in which the cell migration is being tracked. I had performed the tracking from hour 7 to hour 12 after seeding HUVECs onto the scaffolds, but I believe extending the end point to 24 hours after seeding will provide even more information. The reason being that when we fixed the cells after 12 hours and imaged the samples we were able to identify microvascular alignment of the endothelial cells, however, we were not able to see a lumen. Others who have performed similar experiments using the same ECM scaffolds have waited 24 hours prior fixing and imaging and have been able to identify a lumen. While it is evident that the alignment of the endothelial cells occurs after 12 hours, further tracking the cells until the 24 hour time point will provide more information of their motility as they stabilize into vascular networks.

Another advancement I would suggest in the future is to track the endothelial cells in a 3D environment. Although the scaffolds we used mimic the physiological and supportive traits of the microenvironment in vivo, spatial imitation is extremely important when studying pathological processes like angiogenesis. Many researchers have turned to 3D environments to studying such processes and have shown a difference in findings between 2D and 3D. 3D cell migration could lead to significant findings of endothelial cell migration during angiogenesis in the absence of a polymerized fibronectin network.

I believe these suggestions for future work would expand our understanding of angiogenesis and the microenvironment that regulates the process. A deeper knowledge would advance future experiments and contribute to finding an anti-angiogenic therapy to treat cancer.

References

1. Young E.W., *Advances in microfluidic cell culture systems for studying angiogenesis.* J Lab Autom, 2013. **18**(6): p. 427-36.
2. Carmeliet, P., et al., *Branching morphogenesis and antiangiogenesis candidates: tip cells lead the way.* Nat Rev Clin Oncol, 2009. **6**(6): p. 315-26.
3. Griffioen A.W., et al., *Angiogenesis: potentials for pharmacologic intervention in the treatment of cancer, cardiovascular diseases, and chronic inflammation.* Pharmacol Rev, 2000. **52**(2): p. 237-68.
4. Drake, C.J., *Embryonic and adult vasculogenesis.* Birth Defects Res C Embryo Today, 2003. **69**(1): p.73-82.
5. Carmeliet, P., et al., *Molecular mechanisms and clinical applications of angiogenesis.* Nature, 2011. **473**(7347): p. 298-307.
6. Khurana, R., et al., *Role of angiogenesis in cardiovascular disease: a critical appraisal.* Circulation, 2005. **112**(12): p. 1813-24.
7. Carmeliet, P., et al., *Angiogenesis in cancer and other diseases.* Nature, 2000. **14**(6801): p. 249-57.
8. Distler, J.H., et al., *Angiogenic and angiostatic factors in the molecular control of angiogenesis*. Q J Nucl Med, 2003 **47**(3): p. 149-61.
9. Tahergorabi, Z., et al., *A review on angiogenesis and its assays.* Iran J Basic Med Sci, 2012. **15**(6): p. 1110-26.
10. De Falco S., *Antiagiogenesis therapy: an update after ther first decade.* Korean J Intern Med, 2014. **29**(1): p. 1-11.

11. Folkman, J., *Antiangiogenesis in cancer therapy—endostatin and its mechanisms of action.* Exp Cell Res, 2006. **312**(5): p. 594-607.

12. Kostourou V. and Papalazarou V., *Non-collagenous ECM proteins in blood vessel morphogenesis and cancer.* Biochim Biophys Acta, 2014. **14**: p. 79-88.

13. Hynes, R.O., *Extracellular matrix: not just pretty fibrils*. Science, 2009. **326**(5957): p. 1216-9.

14. Rosario, T. and DeSimone, D.W., *The extracellular matrix in development and morphologenesis: a dynamic view.* Dev Biol, 2010. **341**(1): p. 126-40.

15. Lu, P., et al., *Extracellular matrix degradation and remodeling in development and disease.* Cold Spring Harb Perspect Biol, 2011. **3**(12).

16. Afratis, N., et al., *Glycosaminoglycans: key players in cancer cell biology and treatment.* FEBS J, 2012. **279**(7): p. 1177-97.

17. Jin, S.W. et al., *Cellular and molecular analysis o vascular tube and lumen formation in zebrafish*. Development, 2005. **132**(23): p. 5199-209.

18. Kalluri, R., *Basement membranes: structure, assembly and role in tumour angiogenesis*. Nat Rec Cancer, 2003. **422**(3): p. 422-33.

19. Eliceiri, B.P. and Cheresh, D.A., *Adhesion events in angiogenesis.* Curr Opin Cell Bio, 2001. **13**(5): p. 563-8.

20. Hielscher A.C. and Gerecht S., *Engineering approaches for investigating tumor angiogenesis: exploiting the role of the extracellular matrix.* Cancer Res, 2012. **72**(23): p. 6089-96.

21. Kubota, Y., et al., *Role of laminin and basement membrane in the morphological differentiation of human endothelial cells into capillary-like structures.* J Cell Biol, 1988. **107**(4): p. 1589-98.

22. Kim, M.S., et al., *Anti-angiogenic activity of torilin, a sesuiterpene compound isolated from torilis japonica.* Int J Cancer, 2000. **87**(2): p.269-75.

23. Ren, X., et al., *Anti-angiogenic and vascular disrupting effects of C9, a new microtubule-depolymerizing agent.* Br J Pharmacol, 2009. **156**(8): p. 1228-38.

24. Ruggeri, B.A., et al., *The chemopreventive agent oltipraz possesses potent antiangiogenic activity in vitro, ex vivo, and in vivo and inhibits tumor xenograft growth.* Clin Cancer Res, 2002. **8**(1): p. 267-74.

25. Xu, X., et al*., Evaulating dual activity LPA receptor pan-antagonist/autotaxin inhibitors as anti-cancer agents in vivo using engineered human tumors*. Prostaglandins Other Lipid Mediat, 2009. **89**(3-4): p. 140-6.

26. Soucy, P.A. and Romer, L.H., *Endothelial cell adhesion, signaling and morphogenesis in fibroblast-derived matrix.* Matrix Biol, 2009. **28**(5): p. 273-83.

27. Hielscher, A.C., et al., *Breast cancer cell-derived matrix supports vascular morphogenesis.* Am J Physiol Cell Physiol, 2012. **302**(8): p. 1243-56.

28. Franz, M., et al., *Chance in extracellular matrix remodeling and re-expression in fibronectin and tenascin-C splicing variants in human myocardial tissue of the right atrial auricle: implications for a targeted therapy of*

cardiovascular diseases using human SIP format antibodies. J Mol Histol, 2010. **41**(1): p. 39-50.

29. Dallas, S.L., et al., *Dynamics of assembly and reorganization of extracellular matrix proteins.* Curr Top Dev Biol, 2006. **75**: p. 1-24.
30. White, E.S., et al., *New insights into form and function of fibronectin splice variants.* J Pathol, 2008. **216**(1): p. 1-14.
31. Singh, P., et al., *Assembly of fibronectin extracellular matrix.* Annu Rev Cell Dev Biol, 2010. **26**: p. 397-419.
32. Zhou, X., Rowe, R.G., Hiraoka, N., et al., *Fibronectin fibrillogenesis regulates three-dimensional neovessel formation.* Genes Dev, 2008. **22**(9): p. 1231-43.
33. Georges-Labouesse, E.N., et al., *Mesodermal development in mouse embyrons mutant for fibronectin.* Dev Dyn, 1998. **207**(2): p. 145-156.
34. Astrof, S. and Hynes, R.O., *Fibronectins in vascular morphogenesis.* Angiogenesis, 2009. **12**(2): p. 165-75.
35. Chiang, H.Y., et al., *Fibronectin is an important regulator of flow-induced vascular remodeling.* Arterioscler Thromb Vasc Biol, 2009. **29**(7): p. 1074-9.
36. Sottile, J. and Hocking, D.C., *Fibronectin polymerization regulates the compositions and stability of extracellular matrix fibrils and cell-matrix adhesions.* Mol Biol Cell, 2002. **13**(10): p. 3546-3559.
37. Slemeczi, D., et al., *Cell motility as persistent random motion: theories from experiments.* Biophys J, 2005. **89**(2): p. 912-31.

38. Li, S., et al., *Mechanotransduction in endothelial cell migration.* J Cell Biochem, 2005. **96**(6): p. 1110-26.

39. Klemke, R.L., et al., *Regulation of cell motility by mitogen-activated protein kinase.* J Cell Biol, 1997. **137**(2): p. 481-92.

40. Lamalice, L., et al., *Endothelial cell migration during angiogenesis.* Circ Res, 2007. **100**(6): p. 782-94.

41. Harms, B.D., et al., *Directional persistence of EGF-induced cell migration is associated with stabilization of lamellipodial protrusions.* Biophysc J, 2005. **88**(2): p. 1479-88.

42. Stokes, C.L., et al., *Migration of individual microvessel endothelial cells: stochastic model and parameter measurement.* J Cell Sci, 1991. **99**(Pt 2): p. 419-30.

43. Sottile, J. and Chandler, J., *Fibronectin matrix turnover occurs through a caveolin-1-dependent process.* Mol Biol Cell, 2005. **16**(2): p. 757-68.

44. Tomasini-Johansson, B.R., et al., *A 49-residue peptide from adhesion F1 of streptococcus pyogenes inhibits fibronectin matrix assembly.* J Biol Chem, 2001. **276**(26): p. 23430-9.

Resume

KIMBERLY ELLIS

Kellis15@jhu.edu • (781)-640-0251
46 Fosters Ln, Wakefield, MA 01880

EDUCATION

Johns Hopkins University (JHU), Baltimore, MD

MSE, Chemical and Biomolecular Engineering (ChemBE) *May 2014*

BS, Chemical and Biomolecular Engineering *May 2013*
Molecular and Cellular Bioengineering Concentration
Entrepreneurship and Management Minor

Relevant Coursework: Chemical Engineering Product & Process Design, Chemical & Biomolecular Engineering Lab, Modeling Dynamics & Controls, Chemical & Biological Separations, Bioengineering in Regenerative Medicine, Biochemistry, Cellular Biology, Biomaterials I & II, Drug Discovery, Supramolecular Materials & Nanomedicine, Biomacromolecules at the Nanoscale, Pharmaceutical Engineering.

HONORS AND AWARDS

Chemical and Biomolecular Engineering Research Excellence, JHU *2013 & 2012*

Best Product Design, JHU, Senior Process and Design *May 2013*

Best Use of Engineering Concepts in Product Design, JHU *May 2013*

RESEARCH AND ENGINEERING EXPERIENCE

JHU- Gerecht Lab- Vascular Tissue Engineering, Graduate Research Student *Feb 2013–May 2014*
Engineered an extracellular matrix derived from fibroblasts and breast cancer cells to mimic tumor microenvironment. Established a GFP tagged endothelial cell line. Used a fibronectin polymerization inhibitor to study the influence of the fibronectin network on endothelial cell migration during angiogenesis. Performed live-cell, time-lapse confocal microscopy imaging to track the cells' migration. Generated Matlab codes to quantify the migration parameters.

JHU- Senior Process and Product Design, Chemical and Biomolecular Engineering *Jan 2013-May 2013*
Designed an Oral Strip Technology using the protein, Casein, as the active ingredient, and Pullulan as the main polymer to relieve the burning sensation the tongue experiences after consuming spicy foods. Developed a Hot Melt Extrusion manufacturing process with specific conditions based on the stability of Casein and the morphological properties of Pullulan.

JHU- Betenbaugh Lab- Biofuels Engineering, Undergraduate Research Student *May 2011-Jan 2013*
Worked with a strain of algae transfected with a human derived apoptosis inhibitor under several stressful conditions and compared the viability to the unmodified strain of algae.

Brigham & Women's Hospital- Dinulescu Lab- Ovarian Cancer, Research Intern *Jun 2012–Aug 2012*
Studied the synergistic effects of Cisplatin, a chemotherapy drug, and Gamma Secretase Inhibitor on ovarian cancer.

ACTIVITIES

Graduate Student Liaison Committee, Master's Representative *Sep 2013- May 2014*
AICHE Member, American Institute of Chemical Engineers *Sep 2009-May 2014*
Lab Mentor, JHU *Jun 2013- Aug 2013*
Theta Tau Member, Professional Engineering Fraternity *Sep 2010-May 2014*
Club Soccer Player, JHU Women's Club Soccer Team *Sep 2009-May 2014*

SKILLS

Proficient in Matlab, Image J, NIS Elements, Zen, and Microsoft Office.